Rare Metal Materials and Engineering
Volume 41, Suppl. 1, February 2012
Cite this article as: Rare Metal Materials and Engineering, 2012, 41(S1): 341-343.

Evolution of Nanocrystalline TiBCN Structure with Temperature and Mechanism

Chen Xiangyang[1], Ma Shengli[1], Paul K Chu[2]

[1] *State Key Laboratory for Mechanical Behavior of Materials, Xi'an Jiaotong University, Xi'an 710049, China*
[2] *Department of Physics and Materials Science, City University of Hongkong, Kowloon Hongkong, China*

Abstract: Evolution of the $TiB_{0.71}C_{3.32}N_{0.79}$ quaternary nanocomposite structure at 600, 700, 800, 900, and 1000 °C is investigated by high-resolution transmission electron microscopy, X-ray diffraction, X-ray photoelectron spectrometry, and micro-hardness indentation. The nc-Ti(C,N) nanocrystallites exhibit the (200) preferential orientation and the amorphous carbon (a-C) phase gradually transforms into the crystallite graphite phase as the temperature is increased. At 1000 °C, the nc-Ti(C,N) nanocrystallites increase to a size of 13 nm but the microhardness diminishes to 18-19 GPa. The corresponding mechanism is discussed.

Key words: nanocomposites; structure; TiBCN

Quaternary Ti-B-C-N films with high hardness and wear resistance prepared by chemical vapor deposition (CVD) [1], plasma-enhanced CVD [2], and reactive magnetron sputtering (RMS) [3-5] have many industrial applications. The structure is typically a nanocomposite framework composed by nanocrystalline nc-Ti(C, N) embedded in an amorphous a-(C, CN, BN, BC) matrix [1-5]. By introducing different amounts of carbon, boron, and nitrogen, the phase and microstructure can be altered and consequently, the mechanical properties can be enhanced by changing the volume fraction and composition of the amorphous and nanocrystalline phases [5-7]. Recent research activities on Ti-B-C-N nanocomposites have primarily focused on the optimization of the microstructure and mechanical properties by changing the composition. Although thermal processing is an effective way to fine tune the structure and corresponding mechanical properties, its effects on the nc-Ti-B-C-N system have not been studied systematically. In the work reported here, we investigate the thermal evolution of the microstructure and hardness of the Ti-B-C-N nanocomposite system and discuss the associated mechanism.

1 Experiment

The $TiB_{0.71}C_{3.32}N_{0.79}$ films were deposited on high-speed steel substrates by reactive magnetron sputtering using two Ti, two B_4C, and two graphite targets (435 mm×94 mm×8 mm). High purity argon and nitrogen were used as the sputtering gas and reactive gas, respectively. Before deposition, the chamber was evacuated to a base pressure of 3.5×10^{-3} Pa and the samples were sputtered by an Ar plasma for 30 min at −1000 V to clean the surface. The deposition pressure was 3×10^{-1} Pa, bias voltage was −100 V, substrate temperature was 150 °C, nitrogen flow ratio was 2 mL/min, Ti target power, B4C target power, and graphite target power were 2 kW, 1 kW, and 5 kW, respectively.

The samples were heated in a CN61M/ZW-18-22 vacuum furnace at a pressure of 7×10^{-3} Pa to 600, 700, 800, 900, or 1000 °C for 1 h. The composition and elemental chemical states were determined by X-ray photoelectron spectroscopy (XPS, PHI 5802). The crystal structure was determined by D/max-3C X-ray diffraction, and nanocrystalline size was determined using the Scherrer formula and high-resolution microscopy. The microstructure was observed by high- resolution transmission electron microscopy (HR-TEM, JEM-3010). The microhardness of the materials was measured on an MH-5 indentation tester equipped with a Vickers diamond indenter under a load of 25 g to assure that the indentation depth does not exceed 10% of the film thickness (2-3 μm).

2 Results and Discussion

The evolution of the nc-$TiB_{0.71}C_{3.32}N_{0.79}$ structure with temperature is monitored by HR-TEM. Fig.1 displays the fast

Received date: May 25, 2011
Foundation item: Doctorial Subject Special Foundation of Chinese University (20070698087) and Hongkong Research Grants Council (RGC) General Research Funds (CityU 112608)
Corresponding author: Ma Shengli, Professor, State Key Laboratory for Mechanical Behavior of Materials, Xi'an Jiaotong University, Xi'an 710049, P. R. China，Tel: 0086-29-82668395, E-mail: slma@mail.xjtu.edu.cn

Fourier transformation (FFT) spectra and selected area diffraction (SAD) patterns to better understand the phenomenon and mechanism. Fig.1a depicts the microstructure of the as-deposited $TiB_{0.71}C_{3.32}N_{0.79}$ nanocomposite. Nanocrystallites (such as A-C and those cycled by rectangles) with an average size of about 3 nm are surrounded by an amorphous matrix with a thickness of less than 6 nm. The average grain size can be calculated from the full-width at half-maximum (FWHM) value of the corresponding XRD peaks using Scherrer equation [8]. The SAD patterns in Fig.1a show that the three rings belong to the (111), (200), and (220) Bragg reflection of the nanocrystalline Ti(C,N) solid solution, whereas XPS shows that the structure is composed of Ti-N, Ti-C, B-C, sp2B-N, sp2C-C, sp2C-N, and sp3C-N chemical bonds [5]. The amorphous phase comprises amorphous a-(C, CN, BN, BC), and the nano- composite possesses a structure consisting of nano- crystalline nc-Ti(C, N) embedded in an amorphous a-(C, CN, BN, BC) matrix.

Fig.1b shows that almost all the nanocrystallites such as A-D have the {200} lattice fringes and the nano- crystallines are separated by the amorphous matrix after heating at 600 °C. The size of the nanocrystals ranges from 3 to 7 nm with a mean value of 5 nm. In the SAD patterns, the (200) ring becomes stronger than the (111) and (220) rings, confirming that heating to 600 °C spurs the formation of more (200)-oriented nc-Ti(C,N) nanocrystallites. The dim moon-like arcs in the SADP and corresponding lattice fringes show that the lattice spacing (indicated as arrows) is about 0.34 nm, which is consistent with that of graphite {002} shown in JCPDS [8,9]. The amorphous carbon (a-C) phase transforms into the crystallite graphite phase at 600 °C. The FFT spectrum indicates that the diffraction spots become sharper than those of the as-deposited materials further corroborating better crystallization in the nc-Ti(C,N) structure.

However, when the temperature is raised to 1000 °C, the size of the Ti(C, N) nanocrystallites increases obviously to about 13 nm, and high angle grain boundaries can be observed between nanograin A and nanograins B and C. Amorphous grain boundaries less than 1 nm thick can also be observed between nanograin B and nanograin C (Fig. 1c). As shown by the SAD patterns, the width of the (111), (200) and (220) rings become smaller and the (200) ring is stronger than the (111) and (220) ones, suggesting that the Ti(C, N) nanocrystallites become larger but the preferred orientation is still (200).

Fig.2 shows that the evolution of the average nanocrystallite size and hardness as a function of temperature. The nanocrystallite size is determined by averaging the grain size values calculated from the nc-Ti(C,N) (111) and (200) diffraction peaks using the FWHM value of the corresponding XRD peaks and Scherrer equation [10]. At 600-900 °C, the average grain size of the nanocrystallites increases to about 5-6 nm but the hardness does not change significantly. However, at 1000 °C, the mean grain size increases to 13 nm and the hardness diminishes to about 18-19 GPa. It is due to the larger nanocrystallites and can be explained by grain boundary hardening created by the high cohesive energy at the inter-phase boundary which restrains grain boundary sliding. This phenomenon can also be interpreted by the Hall-Petch relationship derived from crystal size refinement [2, 11].

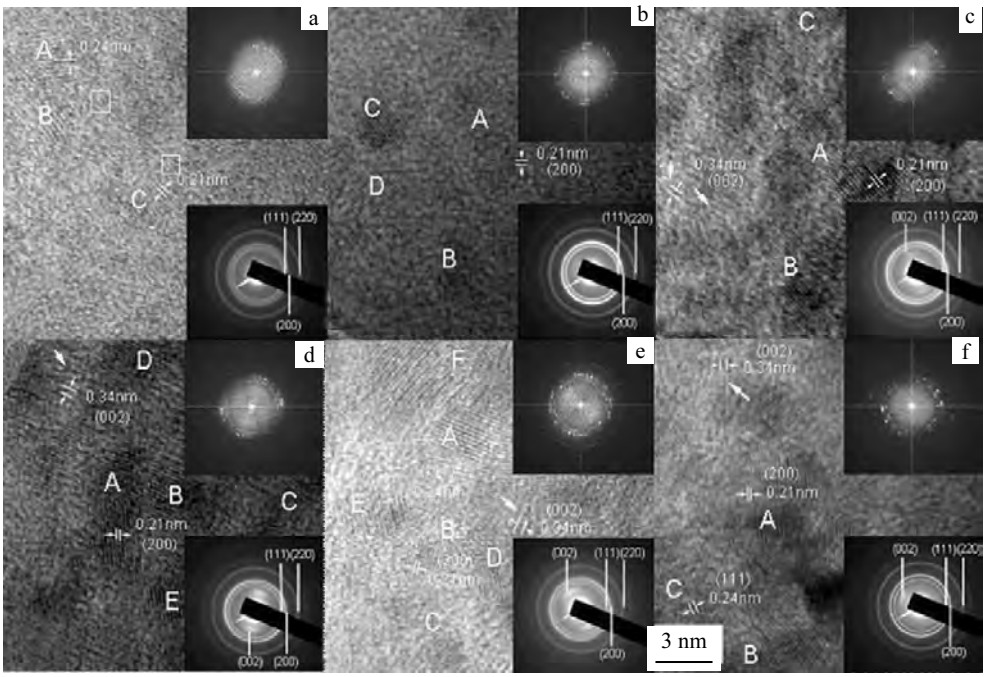

Fig.1 Thermal evolution of the nanocomposite $TiB_{0.71}C_{3.32}N_{0.79}$ structure observed by HR-TEM: (a) As-deposited, (b) 600 °C, (c) 700 °C, (d) 800 °C, (e) 900 °C, and (f) 1000 °C

The results reveal a series of nanocrystallites Ti(C,N) with different sizes and the thermal evolution mechanism from 600 to 1000 °C is postulated as follows. The larger nanograins grow at the expense of the smaller ones and consequently, the average size of the nanocrystallites increases, as shown in Fig.1a, 1b. The growth of the nano- crystallites can be described by the following formula [12]:

$$\mu_i = \frac{2\Omega\gamma}{r_i} \quad (1)$$

where μ_i is the chemical potential, Ω is the atomic volume, γ is the surface tension, and r_i is the radius of the grain. Accordingly, the chemical potential μ_i is inversely proportional to the radii of the nanocrystallines, and so the larger grains have a lower chemical potential. The chemical potential is often associated with the so-called "escaping tendency" of atoms. When r is small, the chemical potential and escaping tendency are large, thus forcing atoms to a region where μ is small [12]. At 1000 °C, the nanograins first grow at the expense of the smaller ones and then the ripened nanograins connect with each other forming larger nanograins in order to reduce the total surface energy of the system

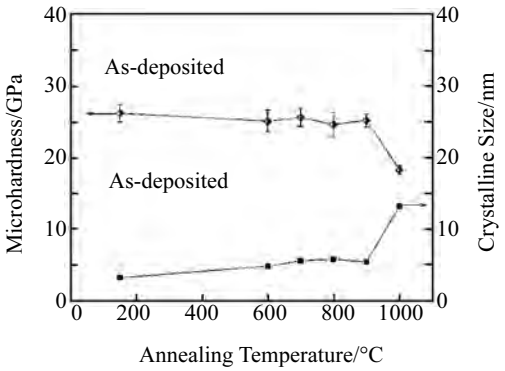

Fig.2 Evolution of grain size and microhardness values as a function

(Fig.1c). In comparison, the thermal evolution mechanism of the carbon phase is probably based on that the unstable amorphous a-C phase transforms into the stable crystalline graphite phase by eliminating the dangling bonds and defect points as suggested previously [13].

3 Conclusions

The $TiB_{0.71}C_{3.32}N_{0.79}$ structure prepared by RMS possesses a nanocomposite structure and at high temperature, the nanocrystallites in the nc-Ti(C,N) exhibit the {200} preferential orientation. As the processing temperature is increased, the amorphous a-C phase gradually transforms into the crystalline graphite phase and at 1000 °C, the average crystallite size increases to 13 nm but the hardness diminishes to 18-19 GPa.

References

1 Shimada S *et al. Surface and Coating Technology*[J], 2007, 201: 7195
2 Kim K H *et al. Surface and Coating Technology*[J], 2006, 201: 4185
3 Mollart T P *et al. Surf Coat Technol*[J], 1996, 86-87: 231
4 Vyas A, Lu Y H, Shen Y G. *Surface and Coating Technology*[J], 2010, 204: 1528
5 Chen Xiangyang *et al. Diamond and Related Materiarials*[J], 2010, 19: 1338
6 Zhong D *et al. Thin Solid Films*[J], 2001, 398-399: 320
7 Lin J *et al. Surface and Coating Technology*[J], 2008, 203: 588
8 Gotoh Y. *Journal of Nuclear Materials* [J], 1997, 248: 46
9 Gupta V *et al. Synthetic Metal* [J], 1995, 73: 69
10 Uvarov V *et al.* M*aterials Characterization* [J], 2007, 58: 883
11 Ma Shengli *et al. Acta Materiala* [J], 2007, 55: 6350
12 Ohring M. *Materials Science of Thin Films*[M]. Singapore: Elsevier, 2006: 395
13 Yang H *et al. Carbon* [J], 2003, 41: 397